Radio Science, Volume 21, Number 5, Pages 845–856, September–October 1986

Airborne measurements of the ocean radar cross section at 5.3 GHz as a function of wind speed

Folkart Feindt,[1] *Volkmar Wismann*,[2] *Werner Alpers*,[3] *and William C. Keller*[4]

(Received October 4, 1985, revised April 25, 1986, accepted April 25, 1986)

Measurements of the normalized radar cross section (NRCS) at 5.3 GHz (C band) of the sea surface as a function of wind speed and direction are presented The data were obtained by a coherent scatterometer mounted on a small two-engine airplane performing circle flights over the Atlantic. Our data show that the wind speed exponent at 5 3 GHz is typically 20% smaller than at 13 9 GHz (K_u band) Furthermore, the upwind/crosswind ratio of the NRCSs at C band is typically 20% smaller, and the upwind/downwind ratio typically 30% smaller than at K_u band

1. INTRODUCTION

Radar backscattering from the ocean surface is determined primarily by the surface roughness. The dominant factor determining the sea surface roughness is the local wind. This fact suggests that it is possible to obtain windfields over the ocean by measuring the normalized radar cross section (NRCS) [*Moore and Fung*, 1979, *Brown*, 1983]. Microwave instruments specifically designed for measuring NRCS's have been flown in space with the aim of obtaining wind information from the world oceans on a quasi-synopstic scale [*Grantham et al.*, 1977; *Brown et al.*, 1982; *Jones et al.*, 1982; *Pierson*, 1983]. Such nonimaging calibrated microwave instruments are called scatterometers. They usually operate at incidence angles where the backscattering is dominated by Bragg scattering, typically between 20 and 70 degrees [*Valenzuela*, 1978]. In order to extract wind information from scatterometer data, the functional dependence of the NRCS on local wind and other environmental parameters must be known. This dependence has been extensively studied at 13.9 GHz which was the microwave frequency band employed by the Skylab scatterometer. A 14.6 GHz scatterometer was flown 1978 on the Seasat A satellite which is known as SASS (Seasat A satellite scatterometer). NASA Langley Research Center installed a 13.9 GHz scatterometer on board a C-130 aircraft (Hercules) and conducted a multiyear measurement program to provide quantitative information on the parametric behavior of the NRCS of the ocean [*Jones et al.*, 1977; *Jones and Schroeder*, 1978; *Schroeder et al.*, 1984]. Their technique consisted in performing circle flights at different bank angles which proved to be a very practicable method of measuring the dependence of the NRCS of the windroughened sea surface on azimuth and incidence angle. These airborne measurements provided the data base for the preflight Seasat scatterometer NRCS wind conversion algorithm [*Schroeder et al.*, 1982; *Jones et al.*, 1982].

The European Space Agency (ESA) is planning to fly in 1990 the first European remote sensing satellite (ERS-1), which will carry a scatterometer operating at 5.3 GHz (C band). However, at present the dependence of the C band NRCS on wind speed and direction is not well known. During the 1960s the Naval Research Laboratory (NRL) in Washington, D. C., made airborne radar backscattering measurements over the sea with a pulsed 4-frequency radar system operating at 8.910 GHz (X band), 4.455 GHz (C band), 1.228 GHz (L band) and 0 428 GHz (P band) [*Guinard et al.*, 1971]. Though these measurements were excellent during that time, they do not provide a reliable basis for optimizing the design of the ERS-1 C band scatterometer nor for developing an algorithm to extract wind information from the ERS-1 scatterometer data.

In this paper we report about our airborne measurements carried out during the ESA C band scatterometer campaign. This was an experiment co-

[1]Institut für Meereskunde, Universität Hamburg, Hamburg, Federal Republic of Germany
[2]Max-Planck-Institut für Meteorologie, Hamburg, Federal Republic of Germany
[3]Fachbereich 1 (Physik), Physik des Meeres, Universität Bremen, Bremen, Federal Republic of Germany.
[4]Naval Research Laboratory, Washington, D. C

Paper number 6S0227
0048-6604/86/006S-0227$08.00

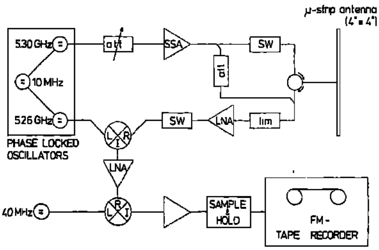

Fig. 1 Block diagram of the coherent pulsed 5.3 GHz scatterometer used in the experiment

ordinated by ESA in which four aircraft from Canada, France, Germany and the Netherlands participated each carrying a different *C* band scatterometer.

Our scatterometer operating at 5.3 GHz at vertical polarization was flown on a small twin-engine propeller airplane (DO-28). The data reported here were collected in February 1984 over the Atlantic off the French coast near Lorient (Brittany).

In this paper we present first results about the dependence of normalized radar cross sections (NRCS) on the wind vector as measured by our instrument during circle flights. Furthermore, we show some evidence that the upwind-crosswind ratio depends on the angle between the wind and swell direction.

2. *C* BAND SCATTEROMETER

A block diagram of the *C* band scatterometer is shown in Figure 1. The scatterometer is a coherent system operating at a frequency of 5.3 GHz. It contains 2 phase-locked oscillators with a difference frequency of 40 MHz and an output power of 30 mW. The transmitted signal of 5.3 GHz is amplified by a solid state amplifier (SSA) of normal 2 W output power and then pulsed by pin-diode switches (SW). The antenna is a planar microstrip antenna (VV polarization) of dimension 1.05 m × 0.95 m with the beam axis squinted electronically 30 degrees downward. The 3-dB one-way half-power beamwidth is 5.2 degrees in elevation and 3.8 degrees in azimuth. The antenna was mounted on the door opening on the left-hand side of the DO-28 without using a radome (Figure 2). The incidence angle could be varied by tilting the antenna. The azimuth angle was fixed such that the antenna looked aft at an angle of 20 degrees (controlled by a goniometer), which provided a Doppler shift induced by the aircraft motion. The backscattered signal is amplified by a low noise amplifier (LNA) and mixed with the 5.260 GHz reference signal of the local oscillator. This intermediate frequency signal is then beaten down to an audio frequency of 40 MHz. The power of the phase-locked oscillator is monitored by coupling a small fraction (−94 dB) of the unpulsed transmitting signal into the receiving channel. This internal calibration signal has zero Doppler shift and can thus be separated from the Doppler shifted ocean signal (see Figure 5).

The scatterometer was operated in the beam-limited mode. The duration of the transmitted pulse was 14 μs and the width of the receiving gate was 1.8 μs. A long pulse was used such that no reprogramming of the pulse sequence was required when changing the altitude of the aircraft. The time delay between transmission and reception was 1.8 μs, which limited the minimum slant range to 420 m. The maximum slant range was 2520 m. The pulse repetition frequency of 38 kHz inclusive the rise time of 1 μs provides a duty cycle of 0.026 ms, which requires a sample and hold device to preserve the output waveform. The data were recorded on an analogue tape-recorder (FM) with a tape speed of 7.5 inches per second corresponding to a bandwidth of 2.5 kHz.

3. THE EXPERIMENT

From Feb. 9 to Feb. 29, 1984, seven flight missions were flown out of the airfield of Lorient over the Atlantic in an area approximately 50 km off the coast of Brittany, France. In this part of the Atlantic the water depth is approximately 100 m.

Circle flights were conducted with a constant bank angle of 18 degrees. Given the aircraft speed of 110 knots a circle was completed in approximately 2 min. Ten circles were flown at a given incidence angle. The incidence angle (angle between nadir and the direction of the antenna beam) was set nominally at 18, 25, 35, 45 and 55 degrees. The flight altitude was 610 m for all flights except for the flights with an incidence angle of 55 degrees where it was 305 m. The total flight duration of one mission was approximately 3 hours. The yaw, pitch and roll (bank) angles of the aircraft were monitored to an accuracy of less than 0.5 degrees.

Simultaneous measurements of the wind speed (at 19.5 m) the air and water temperatures, the omnidirectional wave spectrum and the direction of the swell (measured by ship radar) were performed by

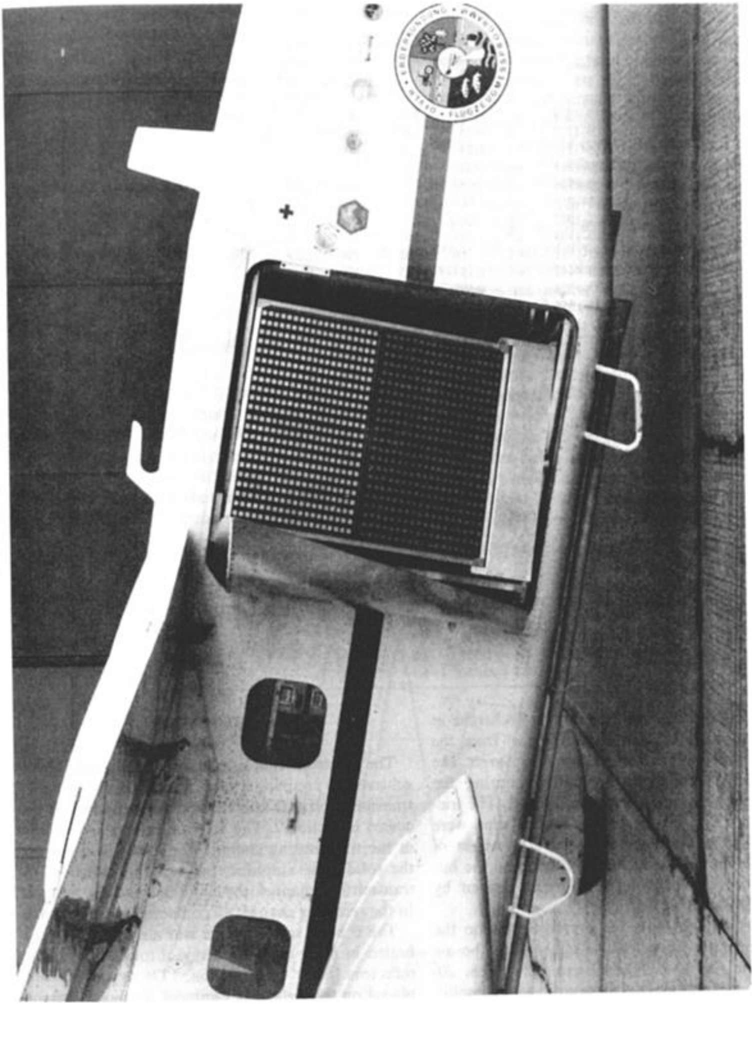

Fig 2 Photograph of the microstrip antenna (dimension, 1.05 m × 0.95 m) mounted in the door opening of the DO-28 aircraft

TABLE 1 Environmental Conditions Encountered During the Flights Over the Atlantic Off the Coast of Brittany, France

		Wind Field				Wave Field		Temperatures	
Date	Time, UT	$U_{19.5}$, m/s	U_*, m/s	$U_{19.5}^{neutral}$, m/s	Direction, °N	H_s, m	Direction, °N	T_{air}, °C	T_{water}, °C
Feb. 9, 1984	1019–1038	8.1	0.268	8.4	005	3.1	300	9.3	11
	1109–1127	7.5	0.25	7.8	003				
	1135–1155	7.1	0.24	7.4	006				
	1200–1211	6.8	0.23	7.1	008				
Feb. 10, 1984	0934–0954	2.2	0.082	2.5	089	1.8	310	8.8	11
	0959–1019	1.8	0.068	2.1	083				
	1022–1042	1.8	0.068	2.1	090				
	1050–1103	1.7	0.065	2.0	102				
Feb 20, 1984	1352–1411	14.5	0.516	14.45	198	3.8	270	11.3	11
	1428–1445	14.8	0.53	14.75	198				
	1507–1524	16.0	0.587	15.96	195				
	1545–1558	15.0	0.573	15.66	197				
	1622–1631	16.4	0.607	16.36	204				
Feb 21, 1984	1052–1111	12.7	0.447	12.96	278	7.1	300	8	10.7
	1121–1140	11.5	0.394	11.76	274				
	1148–1207	12.0	0.416	12.26	251				
	1219–1239	8.4	0.287	8.96	217				
	1248–1307	11.5	0.394	11.76	228				
Feb. 22, 1984	1041–1059	11.4	0.389	11.65	320	5.2	310	8.3	10.8
	1108–1127	12.4	0.433	12.64	324				
	1148–1157	12.2	0.424	12.45	306				
	1207–1226	11.4	0.389	11.65	321				
	1233–1253	11.7	0.402	11.95	304				
Feb 26, 1984	1345–1405	4.9	0.177	5.5	047	1.3	280	4	10.5
	1401–1420	4.9	0.177	5.5	035				
	1433–1450	4.4	0.161	5.0	043				
	1457–1516	3.2	0.121	3.8	047				
	1522–1542	3.1	0.118	3.7	048				
Feb 28, 1984	1006–1022	7.1	0.241	7.5	029	1.1	290	7.2	10.5
	1044–1055	8.3	0.279	8.7	028				
	1102–1121	7.5	0.254	7.9	031				
	1131–1152	7.6	0.257	8.0	029				
	1158–1219	7.7	0.260	8.1	031				

IFREMER (Institut Francais pour la Recherche et L'Exploitation de la Mer, Brest, France) from the French oceanographic research vessel *Le Suroit*. The environmental conditions encountered during the flight missions are summarized in Table 1. The friction velocity U_* and the 19.5 m neutral wind were calculated from the measured wind at a height of 19.5 m, the air and water temperatures, and the humidity of air by applying the formulas given by *Large and Pond* [1981]

During the flight missions over the Atlantic the water temperature was always higher than the air temperature (up to 6 degrees) except for Feb. 20, where the situation was nearly neutral, which implies that the boundary layer at the air-sea interface was always unstable (see Table 1).

4. CALIBRATION

The scatterometer is internally calibrated. This is achieved by coupling a small fraction of the unpulsed transmitted signal into the receiving channel as discussed in section 2 This internal calibration includes in the transmitting channel, the local oscillator and the solid state amplifier, but not the switch of the transmitting channel, the circulator and the antenna In the receiving channel all components are included.

The *C* band scatterometer was also externally calibrated in flight using an array of four 90-cm corner reflectors (radar cross section, 1776 m^2) which were placed on the airfield of Quimper (France). The configuration of the corner reflectors is shown in Figure 3. This configuration was chosen in order to increase

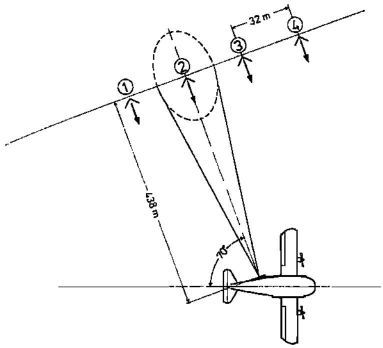

Fig. 3. Configuration of the four corner reflectors used in the calibration flights

the chance of hitting one corner reflector with the antenna beam. Furthermore, this arrangement of corner reflectors allowed us to reconstruct the trace of the beam axis on the ground. The corner reflector overflights were carried out only at low wind speeds ($U \leq 4$ m/s, low air turbulence) such that the flight tracks over the corner reflector could be flown very accurately (no yaw angle deviation from the flight direction).

Figure 4 shows the time history of the backscattered power originating from the four corner reflectors relative to the level of the internal calibration during one calibration flight. By this measurement, cuts through the antenna pattern at 20 degrees off the H plane are obtained. The trace of the beam axis through the array of corner reflectors can be inferred from the relative levels of the four curves. The level of the internal calibration corresponds to a cross section of about 2815 m^2. In the specific example shown in Figure 4, the antenna axis has hit the second corner reflector nearly at the center. In this case, the level of the backscattered power of the second corner reflector is maximum, while the power levels of the two adjacent corner reflectors are nearly equal. Theoretically they should be 0.8 dB lower if the second corner reflector is hit exactly at the center. These measured cuts through antenna pattern agree well with the pattern provided by the manufacturer of the microstrip antenna (Ball Aerospace Corporation)

Furthermore, after each flight over sea, calibration flights were flown over grass lands on the airfield of Quimper, which are distributed targets. This was done in order to intercompare the data sets from the different scatterometers involved in this campaign

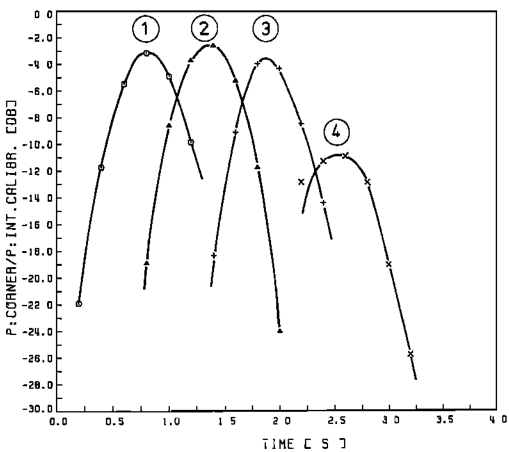

Fig. 4. Backscattered power originating from the four corner reflectors as a function of time. In this calibration flight the second corner reflector was hit by the antenna beam approximately at the center

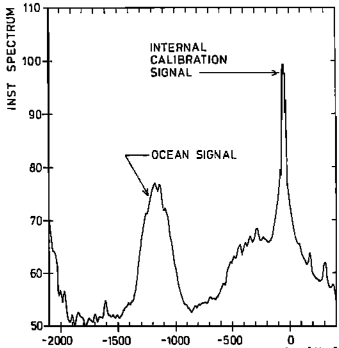

Fig. 5. Doppler spectrum of the return signal from the water surface and the internal calibration signal. The power spectrum is calculated from a total record length of 1.6 s with 16 degrees of freedom. The internal calibration signal has zero Doppler shift.

5. DATA PROCESSING

The analog recorded FM radar output was sampled with a frequency of 5000 Hz for digital processing at the CDC 173 computer. For each segment of 0.2 s duration a power spectrum was calculated with a frequency resolution of 4.9 Hz. Then 8 spectra were averaged corresponding to 1.6 s which amounts to an azimuthal resolution of about 5 degrees, since the flight duration of a full circle was 2 min. Figure 5 shows an example of the averaged power spectrum of the radar output signal. It contains the Doppler shifted signal originating from the water surface and the unshifted internal calibration signal. The signal from the ocean surface has a negative Doppler shift because we used a configuration with a slightly aft looking antenna. For obtaining the radar cross section the spectral energy of the Doppler shifted peak was calculated (integration between the 6 dB points) and divided by the spectral energy of the internal calibration peak. The scatterometer was absolutely calibrated by flying over corner reflectors of known cross section ($\sigma_c = 1776$ m^2).

During the circle flights over water the attitude of the DO 28 was recorded continuously with an accuracy of 0.5 degrees. Especially the roll angle information is very important for later data processing, since the radar cross section depends strongly on the incidence angle. Figure 6 shows one example of the measured crosswind NRCS as function of incidence angle for the flight on Feb. 22, 1984 (wind speed 10–13 m/s, $T_{air} - T_{water} = -2$°C). Such curves were calculated for every flight mission and used for roll angle corrections. All NCRS versus wind speed curves presented in this paper have been corrected for roll and pitch angle variations. The azimuth angle

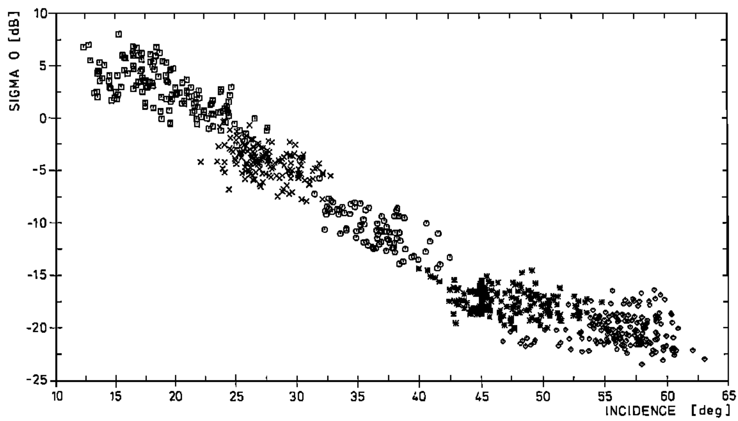

Fig. 6. Variation of the crosswind NRCS at VV polarization with incidence angle as measured during the flight on Feb. 27, 1984 (wind speed, 10–13 m/s, $T_{air} - T_{water} = -2$°C).

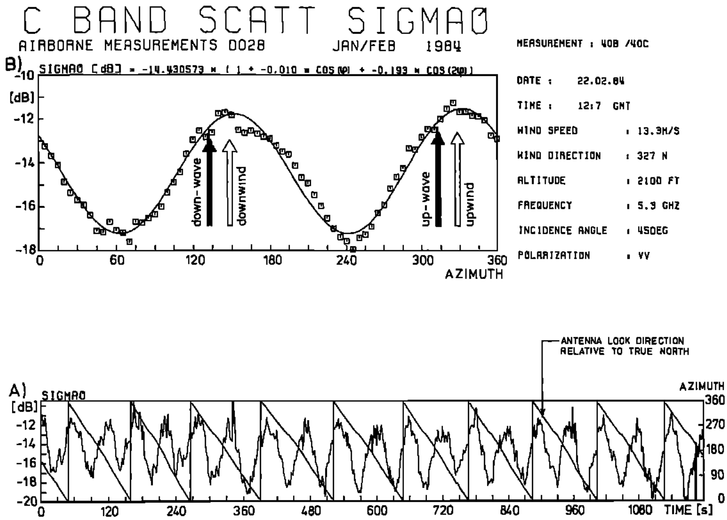

Fig. 7*a*. Typical example of the azimuthal dependence of the *C* band NRCS at VV polarization as measured during circle flights The wind speed was 13 3 m/s The wind was blowing in the direction of the long waves Plot A shows the time series of the measured NRCS together with the antenna look direction relative to true north for 10 circles, and plot B the NRCS averaged other 5 degrees azimuth angle for 10 circle flights The solid line in plot B is a least squares fit to equation (1).

has been calculated from the yaw angle, which was measured continuously on the aircraft by a gyrocompass.

However, we have also processed the data without applying roll angle corrections and by keeping only those data points for which the roll angle deviated by less than 0.5 degrees from its nominal value of 18 degrees. Both methods yield similar results.

6. RESULTS

Two typical examples of the dependence of the NRCS on azimuth angle ϕ (angle between the antenna look direction and true North) measured under different wind and wave conditions are shown in Figures 7*a*, 7*b* Plot A shows the time series of the NCRS as measured during 10 circle flights (total record time: 20 min). The data points shown in plot B represent the NRCS averaged over 5 degrees azimuth angle for the ten circle flights. The wind and swell direction is indicated in the plots by arrows.

As a first step for modelling the functional dependence of the measured NCRS on azimuth angle we use the function

$$\sigma = a(\theta)U^{\gamma(\theta)}(1 + b_1(\theta, U) \cos \phi + b_2(\theta, U) \cos 2\phi) \qquad (1)$$

Here U denotes the wind speed at the height of 19.5 m and a, b_1, b_2 and γ denote fitting parameters, which depend on incidence angle θ. The upwind/crosswind ratio σ_u/σ_c and the upwind/downwind ratio σ_u/σ_d are related to the parameters b_1 and b_2 by

$$\frac{\sigma_u}{\sigma_c} = \frac{1 + b_1 + b_2}{1 - b_2} \qquad (2)$$

$$\frac{\sigma_u}{\sigma_d} = \frac{1 + b_1 + b_2}{1 - b_1 + b_2} \qquad (3)$$

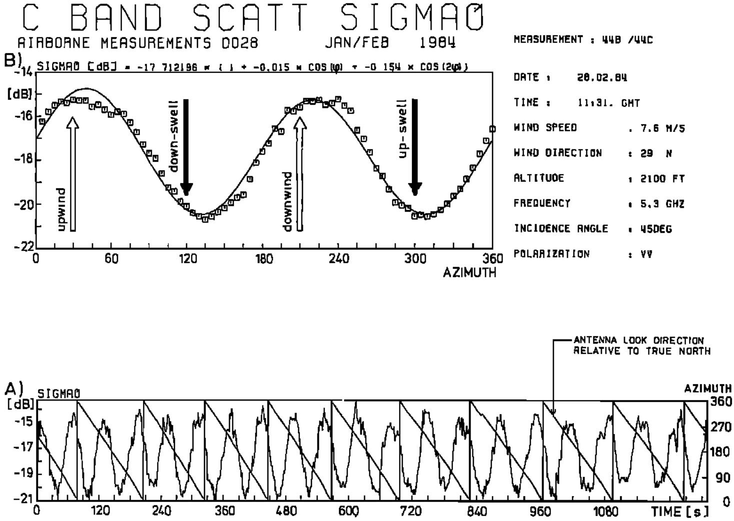

Fig 7b. Same as Figure 7a, but at a wind speed of 7.6 m/s. The swell propagates nearly perpendicular to the wind direction

This model function represents a special case of the model of *Moore and Fung* [1979] and was chosen for its simplicity.

The solid line in Figures 7a, 7b, plot B presents the least squares fit of the measured NRCS to the model curve given by equation (1). In most cases equation (1) fits the measured data quite well. From these least squares fits the wind speed dependence of the NRCS, the upwind/crosswind ratio, and the upwind/downwind ratio of the NRCSs are obtained. Figure 8 shows a plot of the NRCS averaged over all azimuth angles as a function of 19.5 m neutral winds for different incidence angles. The 19.5 m neutral wind was calculated from the measured wind at a height of 19.5 m, the air and sea temperatures and the humidity by applying the formulas given by *Large and Pond* [1981]. In this logarithmic plot of eq (1) the parameter γ ("wind speed exponent") is given by the slope of the curves. γ varies from 1.4 ± 0.2 at 55 degrees incidence angle to 0.7 ± 0.4 at 18 degrees incidence angle. The errors in the wind speed exponents are a consequence of the errors in the NRCS measurements, especially at low wind speeds.

In Figure 9 the NRCS averaged over all azimuth angles is plotted as a function of incidence angle for different wind speeds. These curves give the functional dependence of $\sigma = U^\gamma$ on wind speed and incidence angle (see (1)).

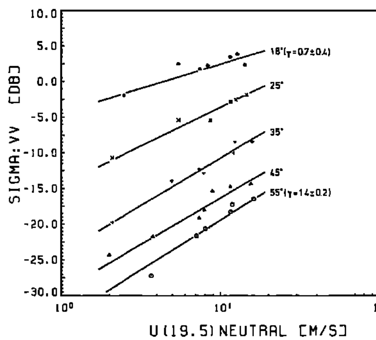

Fig 8 C band NRCS at VV polarization averaged over all azimuth angles as a function of wind speed for different incidence angles

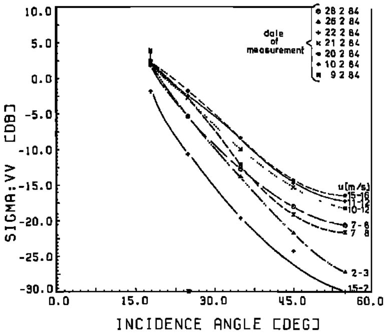

Fig. 9. C band NRCS at VV polarization averaged over all azimuth angles as a function of incidence angle for different wind speeds. Each symbol represents data points of a specific flight mission.

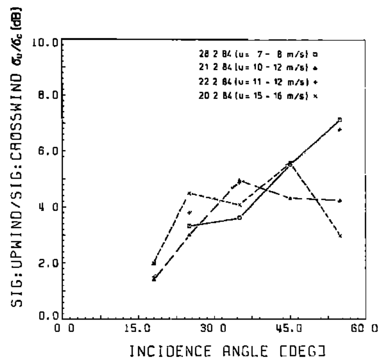

Fig. 11. Upwind/crosswind ratio of the NRCS's as a function of incidence angle for different flight missions. The wind speeds encountered during the missions are given in the figure

The data shown in Figures 8 and 9 are consistent with the assumption that the NRCSs saturate for wind speeds above 10 m/s. But our data base is too small to draw definite conclusions on this controversial issue [*Brown*, 1984].

The upwind/crosswind ratio is shown in Figure 10 as a function of wind speed for three different incidence angles (35, 45 and 55 degrees).

The upwind/crosswind ratio of the NCRSs at 55 degrees lies between 3 and 7 dB, and at 35 and 45 degrees between 2 and 5.5 dB. There is a large scatter in the data points. No systematic dependence of the upwind/crosswind ratio on wind speed can be deduced from our data. This is substantiated further by the fact that σ_u/σ_c was measured differently up to 2 dB on different days, where the wind speed was the same, but the long wave spectrum and the air-sea temperature difference were different.

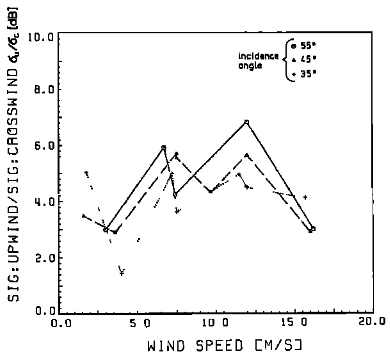

Fig. 10. Upwind/crosswind ratio of the NRCS's as a function of wind speed for three different incidence angles (55, 45 and 35 degrees).

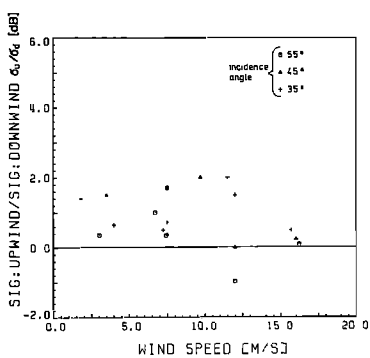

Fig. 12 Upwind/downwind ratio of the NRCS's as a function of wind speed for different incidence angles.

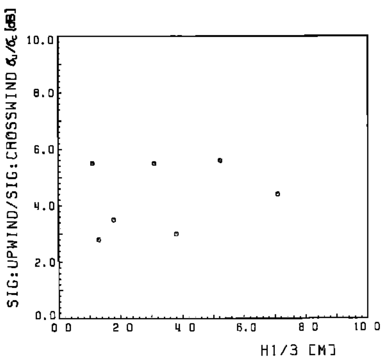

Fig. 13. Upwind/crosswind ratio of the NRCS's as a function of significant wave height H_s

However, our data seem to show a tendency of an increase of the upwind/crosswind ratio with incidence angle in the range between 18 and 35 degrees as can be seen from Figure 11. The scatter of the data points above 35 degrees allows no statement about the incidence angle dependence of the upwind/crosswind ratio.

The upwind/downwind ratio of the NRCSs at 35, 45 and 55 degrees incidence angles as a function of wind speed are shown in Figure 12; σ_u/σ_d varies between 0 and 2 dB as a function of wind speed. No systematic dependence of σ_u/σ_d on wind speed nor incidence angle can be deduced from our data.

The large scatter of the data points seen in Figures 8–12 are certainly not only of statistical origin, but are also caused by variations of other environmental parameters than wind speed and direction. The scatter of the data point could be due in a large part to boundary layer effects in the lower atmosphere and to the underlying long ocean wave field.

A first step in investigating the dependence of the NRCS on the long wave field was done by plotting the upwind/crosswind ratio of the NRCS as a function of significant wave height H_s (Figure 13) and the propagation direction of the long waves relative to the wind direction (Figure 14) for different wind speeds. The long wave field encountered during the experiment over the Atlantic was in most cases not a wind sea but a swell. No dependence on H_s can be deduced from Figure 13.

However, from Figure 14 a dependence of the upwind/crosswind ratio on the angle may be inferred. The upwind/crosswind ratio is largest when the wind blows into the direction of the waves ($\phi_s = 0°$) and decreases when it blows at any other angle to the waves (swell). However, in order to convert this ten-

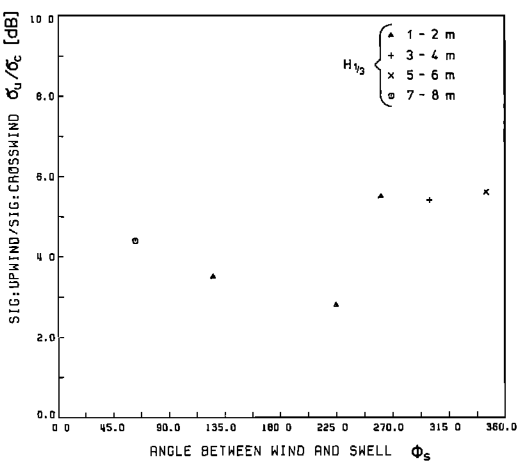

Fig 14. Upwind/crosswind ratio of the NRCS's as a function of the angle between wind and swell direction.

TABLE 2 Summary of the Measured Radar Cross Sections

Date	Time, UT	Incidence Angle θ, deg	$\bar{\sigma}$, dB	σ_u, dB	σ_d, dB	σ_c, dB
Feb 9, 1984	1019–1038	18	+2.3	·	··	··
	1109–1127	35	−12.2	−10.0	−11.0	−14.1
	1135–1155	45	−19.1	−15.6	−16.3	−21.2
	1200–1211	55	−21.6	−18.9	−19.6	−25.3
Feb. 10, 1984	0934–0954	18	−1.9	−0.2	−0.5	−4.1
	0959–1019	25	−10.7	−8.7	−8.8	−12.7
	1022–1042	35	−19.7	−17.1	−17.5	−21.5
	1050–1103	45	−24.3	−21.9	−22.6	−27.5
Feb. 20, 1984	1352–1411	18	+2.4	+4.4	+3.1	+0.9
	1428–1445	25	−1.8	+0.6	+0.0	−4.4
	1507–1524	35	−8.4	−5.8	−6.6	−10.8
	1545–1558	45	−14.3	−13.3	· ·	−18.8
	1622–1631	55	−16.4	−13.6	−15.0	−18.5
Feb 21, 1984	1052–1111	18	+3.9	+4.9	+4.3	+3.5
	1121–1140	25	−2.8	−1.2	−1.6	−3.7
	1148–1207	35	−10.0	−7.5	−8.6	−11.7
	1219–1239	45	−15.3	−12.9	−14.4	−17.0
	1248–1307	55	−18.2	−15.4	−15.6	−20.2
Feb 22, 1984	1041–1059	18	+3.5	+4.3	+4.2	+2.5
	1108–1127	25	−2.5	−0.8	−0.9	−4.2
	1148–1157	35	−8.4	−6.1	−6.9	−11.5
	1207–1226	45	−14.7	−12.0	−12.0	−18.3
	1233–1253	55	−17.2	−13.9	−14.6	−23.4
Feb. 26, 1984	1345–1405	18	+2.5	+3.2	+2.8	+1.7
	1401–1420	25	−5.4	−4.3	−4.9	−6.1
	1433–1450	35	−13.9	−12.8	−13.5	−14.7
	1457–1516	45	−21.7	−19.8	−20.8	−23.2
	1522–1542	55	−27.2	−25.2	−26.0	−28.5
Feb 28, 1984	1006–1022	18	+1.8	+2.9	+2.4	+0.3
	1044–1055	25	−5.4	−3.4	−4.3	−6.8
	1102–1121	35	−12.8	−11.1	−11.5	−14.8
	1131–1152	45	−18.0	−15.3	−15.8	−21.6
	1158–1219	55	−20.6	−17.2	−18.5	−24.7

tative result into a definite one, more data points are needed

In Table 2 the results of the radar cross section measurements are summarized; $\bar{\sigma}$ denotes the normalized radar cross section (NRCS) averaged over all azimuth angles, and σ_u, σ_d, and σ_c the upwind, downwind, and crosswind NRCSs, respectively.

7 DISCUSSION

A comparison of the wind speed exponent measured in our C band experiment with the wind speed exponents measured previously by other investigators with airborne scatterometers operating 0.428 GHz (P band), 1.228 GHz (L band), 8.910 GHz (X band), 10.00 GHz (X band), 13.9 GHz (K band), and 34.4 GHz (K_a band) is shown in Figure 15. The measurements at the first four frequencies were car-

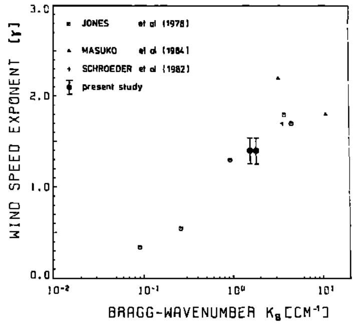

Fig. 15. The 19.5 m wind speed exponent γ as a function of Bragg wave number k_B for vertical polarization and upwind direction. The open dots represent data obtained by *Jones and Schroeder* [1978], the crosses represent the SASS model data [*Schroeder et al.*, 1982] and the open triangles data obtained by *Masuko et al.* [1985], while the solid dots with the error bar are our data points measured at C band

ried out by the Naval Research Laboratory [*Guinard et al.*, 1971; *Daley*, 1973], the measurements at 13.9 GHz by NASA Langley Research Center [*Jones and Schroeder*, 1978; *Schroeder et al.*, 1982, 1984] and the ones at 10.0 GHz and 34.4 GHz by a Japanese group [*Masuko et al.*, 1985]. In Figure 15 the wind speed exponent is plotted as a function of the Bragg wave number k_B which is defined by $k_B = (4\pi/c)f \sin\theta$.

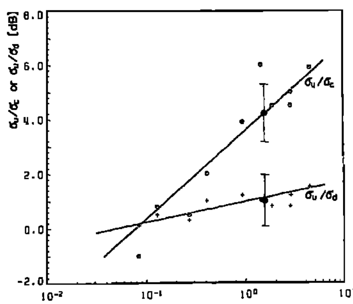

Fig. 16 Upwind/crosswind and upwind/downwind ratios of the NRCS's as a function of Bragg wave number k_B. The open dots and crosses represent data obtained by *Jones and Schroeder* [1978], while the solid dots with the error bar represent our data points measured at C band

Here c denotes the speed of light, f the radar frequency and θ the angle between nadir and the radar antenna axis (incidence angle). The data points marked by open circles in Figure 15 are taken from the paper of *Jones and Schroeder* [1978], which also contains the data obtained by the Naval Research Laboratory four-frequency radar.

This figure suggests that the wind speed exponent increases with Bragg wave number. The wind speed exponent obtained from our measurements at C band is 1.4 at $\theta = 55°$. The exponent measured by *Schroeder et al.* [1984] at K_u band (13.9 GHz) is 1.73 at $\theta = 50°$. This result implies that the planned ERS-1 scatterometer operating at C band would be about 20% less sensitive than the K_u band scatterometer flown on Seasat [*Schroeder et al.*, 1982].

A comparison of the upwind/crosswind and upwind/downwind ratios of the NRCS's measured in our C band experiment with the ratios measured at other frequencies [*Jones and Schroeder*, 1978] is shown in Figure 16. Our data points at C band seem to fit quite well into the curves given by *Jones and Schroeder* [1978]. However, it should be kept in mind that in our experiment the measured ratios exhibit a large scatter, which might be due to the influence of the ocean wave field or other environmental parameters. The curves of Figure 16 show that the upwind/crosswind ratio increases strongly, and the upwind/downwind ratio increases weakly with the Bragg wave number k_B.

The upwind/crosswind ratio of the NRCS at C band is approximately 1 dB smaller than at K_u band, and the upwind/downwind ratio at C band is 0.5 dB smaller than at K_u band.

Our measurements clearly indicate that the NRCS is not uniquely related to the wind speed, but depends also on other environmental parameters like long wave slope. This needs further investigation.

Acknowledgments. This experiment was carried out as part of the ESA 1984 C band scatterometer campaign. It was supported by the European Space Agency and the Bundesministerium für Forschung und Technologie We thank R. Ezraty of IFREMER, Brest, France, for providing the meteorological and oceanographic data Furthermore, we thank J C Morin of ESA, H. Finkenzeller of the DFVLR, and the crew of the DO-28 aircraft, P. Vogel and G Kumbier, for their engaged collaboration.

REFERENCES

Brown, R. A, On a satellite scatterometer as an anemometer, *J Geophys Res.*, *88*, 1663–1673, 1983

Brown, R. A., Scatterometer capabilities in remotely sensing geophysical parameters over the ocean The status and the possibilities, Proceedings of the URSI Commission F Symposium "Frontiers of Remote Sensing of the Oceans and Troposphere from Air and Space Platforms," Shoresh, Israel, May 13–14, 1984, *NASA Conf Publ*, *2303*, 51–55, 1984

Brown, R. A, V. J. Cardone, T. Guymer, J. Hawkins, J. E. Overland, W. J Pierson, S. Peteherych, J C Wilkerson, P. M Woiceshyn, and M Wurtele, Surface wind analyses for SEASAT, *J. Geophys. Res.*, *87*(C5), 3355–3364, 1982

Daley, J, Wind dependence of radar sea return, *J Geophys Res*, *78*, 7823–7833, 1973

Grantham, W L, E. M Bracalente, W. L Jones, and J. W Johnson, The SEASAT-A satellite scatterometer, *IEEE J. Oceanic Eng*, *OE-2*, 200–206, 1977.

Guinard, N. W, J. T Ransone, and J C. Daley, Variation of the NCRS of the sea with increasing roughness, *J Geophys. Res.*, *76*, 1525–1538, 1971.

Jones, W., and L. C. Schroeder, Radar backscatter from the ocean: Dependence on surface friction velocity, *Boundary Layer Meteorol.*, *13*, 133–149, 1978

Jones, W L., L C. Schroeder, and J L Mitchell, Aircraft measurements of the microwave scattering signature of the ocean, *IEEE J Oceanic Eng.*, *OE-2*, 52–61, 1977.

Jones, W. L, L C Schroeder, D H Boggs, E M Bracalente, R. A. Brown, G. J. Dome, W J. Pierson, and F. J Wentz, The SEASAT-A satellite scatterometer: The geophysical evaluation of remotely sensed wind vectors over the ocean, *J Geophys Res.*, *87*(C5), 3297–3317, 1982

Large, W G., and S Pond, Open ocean momentum flux measurements in moderate to strong winds, *J. Phys Oceanogr.*, *11*, 324–336, 1981.

Masuko, H, K Okamoto, T. Takasugi, M. Shimada, H. Yamada, and S Niwa, Experimental results of sea-surface scattering by airborne microwave scatterometer/radiometer, in *The Ocean Surface, Wave Breaking, Turbulent Mixing and Radio Probing*, edited by Y. Toba and H. Mitsuyasu, pp. 319–327, D. Reidel, Hingham, Mass., 1985

Moore, R K, and A. K. Fung, Radar determination of winds at sea, *Proc IEEE*, *67*, 1504–1521, 1979

Pierson, W J., Highlights of the SEASAT-SASS program. A review, in *Satellite Microwave Remote Sensing*, edited by T D Allan, pp 69–86, Ellis Horwood Limited, Chichester, England, 1983

Schroeder, L C, D H. Boggs, G. Dome, I. M. Hallerstam, W L Jones, W. J. Pierson, and F J Wentz, The relationship between wind vector and normalized radar cross-section used to derive SEASAT-A scatterometer winds, *J. Geophys. Res.*, *87*(C5), 3318–3336, 1982.

Schroeder, L. C., W L Jones, P. R. Schaffner, and L Mitchell, Flight measurement and analysis of AAFE RADSCAT wind speed signature of the ocean, *NASA Tech Memo*, *85646*, 144 pp., 1984

Valuenzuela, G. R., Theories for the interaction of electromagnetic and ocean waves—A review, *Boundary Layer Meteorol.*, *13*, 61–85, 1978

W. Alpers, Fachbereich 1 (Physik), Physik des Meeres, Universität Bremen, 2800 Bremen 33, Federal Republic of Germany

F Feindt, Institut für Meereskunde, Universität Hamburg, 2000 Hamburg 13, Federal Republic of Germany

W. C Keller, Naval Research Laboratory, Washington, DC 20375.

V Wismann, Max-Planck-Institut für Meteorologie, Bundestrasse 55, 2000 Hamburg 13, Federal Republic of Germany.